ACS OMEGA

http://pubs.acs.org/journal/acsodf

Article

Electrophoretic Deposition, Microstructure, and Selected Properties of Poly(lactic-*co*-glycolic) Acid-Based Antibacterial Coatings on Mg Substrate

Jawad Manzur, Memoona Akhtar, Aqsa Aizaz, Khalil Ahmad, Muhammad Yasir, Badar Zaman Minhas, Egemen Avcu, and Muhammad Atiq Ur Rehman*

Cite This: *ACS Omega* 2023, 8, 18074−18089

Read Online

ACCESS | Metrics & More | Article Recommendations | Supporting Information

ABSTRACT: There is an urgent need to develop biodegradable implants that can degrade once they have fulfilled their function. Commercially pure magnesium (Mg) and its alloys have the potential to surpass traditional orthopedic implants due to their good biocompatibility and mechanical properties, and most critically, biodegradability. The present work focuses on the synthesis and characterization (microstructural, antibacterial, surface, and biological properties) of poly(lactic-*co*-glycolic) acid (PLGA)/henna (*Lawsonia inermis*)/Cu-doped mesoporous bioactive glass nanoparticles (Cu-MBGNs) composite coatings deposited via electrophoretic deposition (EPD) on Mg substrates. PLGA/henna/Cu-MBGNs composite coatings were robustly deposited on Mg substrates using EPD, and their adhesive strength, bioactivity, antibacterial activity, corrosion resistance, and biodegradability were thoroughly investigated. Scanning electron microscopy and Fourier transform infrared spectroscopy studies confirmed the uniformity of the coatings' morphology and the presence of functional groups that were attributable to PLGA, henna, and Cu-MBGNs, respectively. The composites exhibited good hydrophilicity with an average roughness of 2.6 μm, indicating desirable properties for bone forming cell attachment, proliferation, and growth. Crosshatch and bend tests confirmed that the adhesion of the coatings to Mg substrates and their deformability were adequate. Electrochemical Tafel polarization tests revealed that the composite coating adjusted the degradation rate of Mg substrate in a human physiological environment. Incorporating henna into PLGA/Cu-MBGNs composite coatings resulted in antibacterial activity against *Escherichia coli* and *Staphylococcus aureus*. The coatings stimulated the proliferation and growth of osteosarcoma MG-63 cells during the initial incubation period of 48 h (determined by the WST-8 assay).

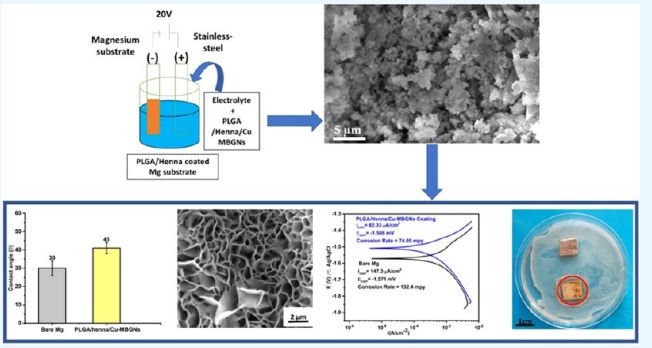

1. INTRODUCTION

The orthopedic implant market is projected to reach US 363.43 billion dollars by 2032 due to aging and chronic diseases.[1−3] First-generation biomaterials (the 1960s to the 1980s) favored bioinert materials to reduce the risk of toxicity. Second-generation biomaterials focus on implant and host tissue interaction (bioactive materials). Metallic implants lack cellular interaction with the host tissue, which can be addressed by depositing biocompatible coatings on metallic implants, such as chitosan, alginate, gelatin, hydroxyapatite (HA), and bioactive glasses (BGs).[4−6] These biomaterials required bioactivity and biodegradability. Specifically, biodegradable implants can lower the stress-shielding effect and eliminate the need for subsequent surgeries to remove nonbiodegradable metallic implants, such as titanium alloys and stainless steel.[4] Commercially pure magnesium (Mg) and its alloys have the potential to surpass traditional orthopedic implants due to their good biocompatibility, mechanical properties, and, most critically, biodegradability.[7,8] In a few instances, however, Mg-based implants failed prematurely due to rapid corrosion and high hydrogen evolution.[9,10] In addition, the uncontrolled release of metallic ions due to the degradation of metallic implants may cause serious health problems.[11]

The dissolution rate of pure Mg implants under in vitro conditions is reported as 407 mm/year.[12] The therapeutic amount of Mg in the body is 55−75 mg/L.[13] However, if Mg is left unchecked, it can have hazardous effects on the body. At 200 mg/L, the body will experience muscle weakness and loss of reflexes in tendons. At 260 mg/L, there are signs of

Received: March 1, 2023
Accepted: April 28, 2023
Published: May 10, 2023

abnormal surface conductivity, and the body starts experiencing respiratory paralysis. At above 450 mg/L, the body begins to undergo cardiac arrest.[14] Therefore, it is imperative to regulate the degradation rate of Mg implants. To address this issue, it is crucial to develop biodegradable orthopedic implants that promote osteogenesis and degrade at a controlled rate. Surface coatings on Mg implants improve bioactivity and reduce the corrosion rate. Metallics implants can be coated via various techniques such as electrophoretic deposition (EPD), plasma spray-coating, laser deposition, and wet methods (sol−gel-based spin-and-dip or spray-coating deposition).[15−17] Among them, EPD is a versatile and low-cost technique that can deposit coatings on complex three-dimensional (3D) shapes,[18] which can deposit thin films to enhance the substrate's mechanical, chemical, and biological properties.[14] Thus, the present study uses EPD to deposit poly(lactic-*co*-glycolic) acid (PLGA)/henna (*Lawsonia inermis*)/Cu-doped mesoporous bioactive glass nanoparticles (Cu-MBGNs)-based coatings on Mg substrates.

Due to their higher chemical reactivity, the new BGs, also known as mesoporous bioactive glass nanoparticles (MBGNs), can provide better bioactivity and therapeutic effects. MBGNs are the new generation of conventional BGs, which exhibit a higher surface area and pore size.[7] Thus, MBGNs can be doped with a variety of metallic ions owing to the intrinsic porosity (usually MBGNs exhibit a pore size of 2−7 nm) in their texture, which can provide a therapeutic effect. For example, Cu, Ag, Mn, Sr, etc., can induce angiogenesis, antibacterial activity, enhanced osteoblast proliferation, and improved bioactivity.[7,19] Even without any doping, MBGNs properties could enhance the mineralization ability and pulp cell behavior.[17]

In the present study, Cu-MBGNs were utilized to provide antibacterial and angiogenesis effects.[20] PLGA is formed by the ring-opening copolymerization of lactic ($C_3H_6O_3$) and glycolic acids ($C_2H_4O_3$), which can provide biocompatibility and controlled biodegradability to Mg-based implants.[18,19] Natural herbs such as mint, oregano, and henna provide antimicrobial properties.[21] In addition, it is widely acknowledged that natural herbs are safer than antibiotics.[22] Herbal compounds can be loaded with biopolymers for targeted drug delivery at the site of infection, which are more efficient than oral drug administration.[23] More particularly, henna, a flowering plant scientifically known as *L. inermis* ($C_{10}H_6O_3$),[24] has antibacterial activity and a broad spectrum of biological activity due to its chemical structure containing 2-hydroxy-1,4-naphthoquinone.[25] Therefore, the present study incorporates henna and Cu-MGBNs into the PLGA matrix to enhance antibacterial activity and promote angiogenesis.

Thus far, nanohydroxyapatite (nHA) and poly(lactide-*co*-glycolide) (PLGA) composite coatings have been successfully deposited on Mg substrates using EPD.[26] Also, PLGA coatings on Mg substrates have been shown to improve biocompatibility and corrosion resistance.[27] In another study, PLGA coatings on Mg substrates have been shown to prevent stress corrosion cracking.[28] Curcumin-loaded PLGA nanoparticle coatings have also been deposited on 316 L stainless steel substrates.[29] More recently, Mahmood Razzaghi et al.[30] have introduced PLGA/hardystonite composite coatings on Mg−3Zn−0.5Ag−15NiTi nanocomposites for potent antibacterial effect and in vitro bioactivity. However, the existing literature on the incorporation of natural herbs and Cu-MBGNs into the PLGA matrix and the deposition of these composite coatings is very limited. Most importantly, PLGA/henna/Cu-MBGNs coatings on Mg substrates have yet to be investigated.

To the best of the authors' knowledge, this is the first time PLGA/henna/Cu-MBGNs were coated on Mg substrates using EPD. The aim of this study was to develop a composite coating having antibacterial effect and bioactivity with suitable corrosion resistance. It was hypothesized that the presence of PLGA in the composite coatings can reduce the corrosion rate. Furthermore, the incorporation of henna is expected to provide an antibacterial effect. The addition of Cu-MBGNs in the composite coatings is expected to improve the osteointegration of the metallic implant. To explore the different characteristics of the coatings, analytical, electrochemical, and biological analyses were performed.

2. MATERIALS AND METHODS

2.1. Materials. Pure magnesium sheets (Science Centre, Pakistan) in the rolled form with a purity of ∼99.98% were purchased. Poly(glycolic acid) (100% pure, M_W = 10,1000), *N*,*N*-dimethyl formamide (DMF), poly(lactic acid) (100% pure, M_W = 10,1000), deionized water, glacial acetic acid, absolute ethanol, tetraethyl orthosilicate (TEOS) 99% pure, calcium nitrate ($Ca(NO_3)_2{\cdot}4H_2O$) 98% pure, ethyl acetate 99.8% pure, cetyltrimethylammonium bromide (CTAB), copper nitrate ($Cu(NO_3)_2$), and ammonium hydroxide (NH_4OH) were used in this study. All chemicals used were of analytical grade and purchased from Sigma-Aldrich.

2.2. Sample Preparation. Mg substrates were cut into rectangular (10 mm × 30 mm) and disc (diameter of 13 mm and a thicknesses of 2−3 mm) shapes. The disc-shaped samples were utilized for cell culture studies, and all other material characterizations were carried out on the rectangular-shaped samples. The samples were cut into the required shape by using electrical discharge machining (EDM). After cutting, the samples were then polished with 600−800 grit SiC sandpapers. The sandpapers were regularly sprayed with a grinding solution of ethanol and glycerol (3:1) to prevent overheating of the Mg substrates. The substrates were polished three times for 2 min with cotton cloths and three distinct diamond suspensions with particle sizes, i.e., 6, 3, and 1 μm. During polishing, a lubricant comprising ethanol and neutral soap was utilized. The substrates were then placed in an ultrasonic bath of ethanol for 5 min to remove any remaining polishing residue. The substrates were then rinsed with fresh ethanol and dried in hot air.[31] The substrates were then subjected to a chemical treatment, as described elsewhere.[32]

2.3. PLGA Synthesis. The PLGA copolymer was synthesized via a ring-opening polycondensation reaction between lactic acid and glycolic acid, as shown in Figure 1. Optimal concentrations were chosen to prepare the solution by following a previous study.[33] Poly(lactic acid) (PLA) and poly(glycolic acid) (PGA) were mixed in a ratio of 75/25 under continuous stirring at 30 °C for 20 min. PLGA (a brown sticky substance) was formed when 2 mL of a cross-linking agent, i.e., DMF, was added to the solution. Then, it was stirred at 120 °C for 8 h. After PLGA was synthesized, henna ($C_{10}H_6O_3$) was added to PLGA to impart antibacterial properties to the composite coatings.

2.4. Synthesis of Cu-MBGNs. The modified Stöber process was used to prepare Cu-MBGNs, as specified by Bano et al.[34,35] First, 0.56 g of CTAB was dissolved in deionized water at 40 °C under constant stirring. Then, 8 mL of ethyl acetate was slowly added to the homogeneous

https://doi.org/10.1021/acsomega.3c01384
ACS Omega 2023, 8, 18074−18089

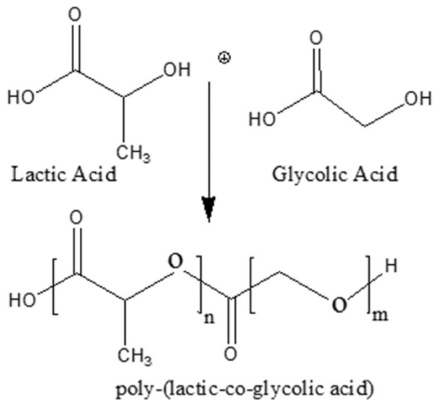

Figure 1. Chemical reaction between lactic acid and glycolic acid to form poly(lactic-*co*-glycolic) acid.

solution. The catalyst, i.e., 0.3 mL of NH_4 OH (32 vol %), was first diluted in deionized water before being added to maintain a pH of ∼10. Next, the precursor of silica particles, TEOS, was added dropwise to the solution under continuous stirring. Next, the Cu-containing salt, i.e., 0.1925 g of copper nitrate, was added to the solution under constant stirring for 30 min to prepare 7 mol % Cu-MBGNs. The solution was stirred overnight for the reaction to occur. After that, the suspension was centrifuged at ∼8000 rpm for 10 min to precipitate the particles. Then, the particles were washed with water and ethanol 3 times. Finally, the particles were dried in an oven at 70 °C for 12 h and calcinated at 700 °C for 5 h to eliminate all nitrates of precursors used during synthesis.[35] Figure 2 schematically illustrates the synthesis of Cu-doped MBGNs. The concentration of Cu in MBGNs was chosen based on a previous study.[20] The nominal composition of Cu-MBGNs was $70SiO_2$−23CaO−7CuO (mol %).

2.5. Suspension Preparation. In order to prepare the suspension for PLGA/henna/Cu-MBGNs composite coatings, 8 vol % PLGA, 2 g/L henna, and 2 g/L Cu-MBGNs were added to a solution containing 10 mL of acetic acid and 3 mL of distilled water. Afterward, the solution was stirred for 30 min. Later, 37 mL of absolute ethanol was added to the solution and stirred for 30 min, followed by ultrasonication. The pH of the suspension was maintained at ∼4 by adding dropwise acetic acid.[2]

The amount of henna was chosen based on some preliminary experimental work, suggesting that if the concentration of henna is <2 g/L, the antibacterial effect subsided.[25] In addition, the concentration of Cu-MBGNs was determined considering the fact that the suspension was not stable above 2 g/L Cu-MBGNs. Furthermore, if the concentration in the suspension is <2 g/L, then the bioactivity will be compromised.[36] Consequently, the suspension properties and implemented deposition parameters are listed in Table 1.

Table 1. Suspension Properties and EPD Parameters Used for Depositing PLGA/Henna/Cu-MBGNs Composite Coatings on Mg Substrates

materials and composition of the 50 mL suspension		EPD parameters	
PLGA	8 vol % (pure 100 5, M_W = 1,010,000)	applied voltage	20 V
Cu-MBGNs	2 wt %	deposition time	7 min
henna	2 wt %	interelectrode distance	10 mm
ethanol	74 vol %	substrate	magnesium
distilled water	6 vol %		
acetic acid	20 vol %		

2.6. Electrophoretic Deposition. EPD was utilized to deposit PLGA/henna/Cu-MBGNs onto Mg substrates (cathode). Mg substrate was used as the cathode (deposition electrode), and 316 L stainless steel (316 L SS) was used as the counter electrode (anode). Electrodes were connected to the power supply through Cu wires. The interelectrode spacing was set at 10 mm. A DC power supply (ETM-605) was used to generate a constant current. In the case of rectangular samples, the coated area was 10 mm × 15 mm. However, in the case of disc-shaped samples, the whole area was coated (for cell culture studies). Only the coated area was subjected to the relevant material characterization. The deposition time and

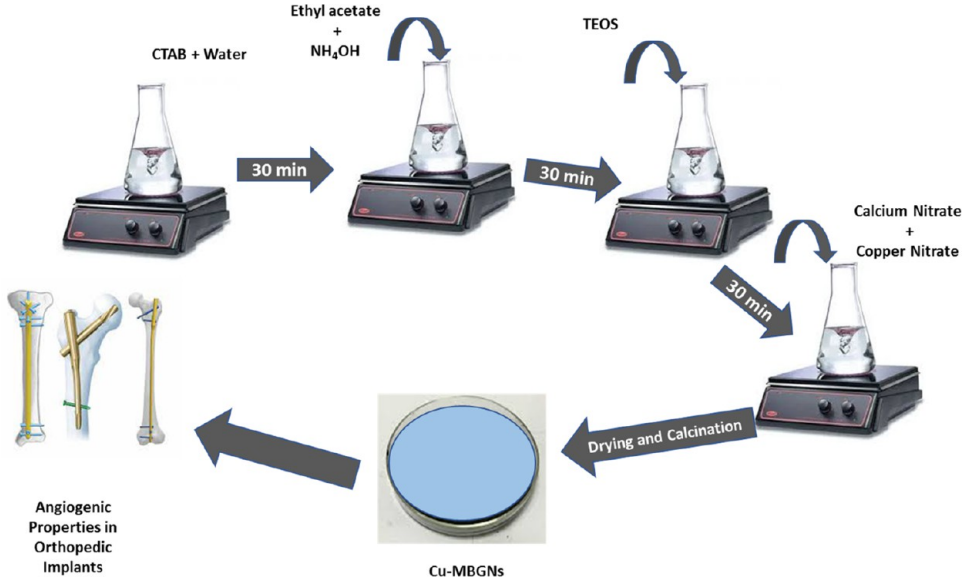

Figure 2. Schematic illustration of the synthesis of Cu-MBGNs.

https://doi.org/10.1021/acsomega.3c01384
ACS Omega 2023, 8, 18074−18089

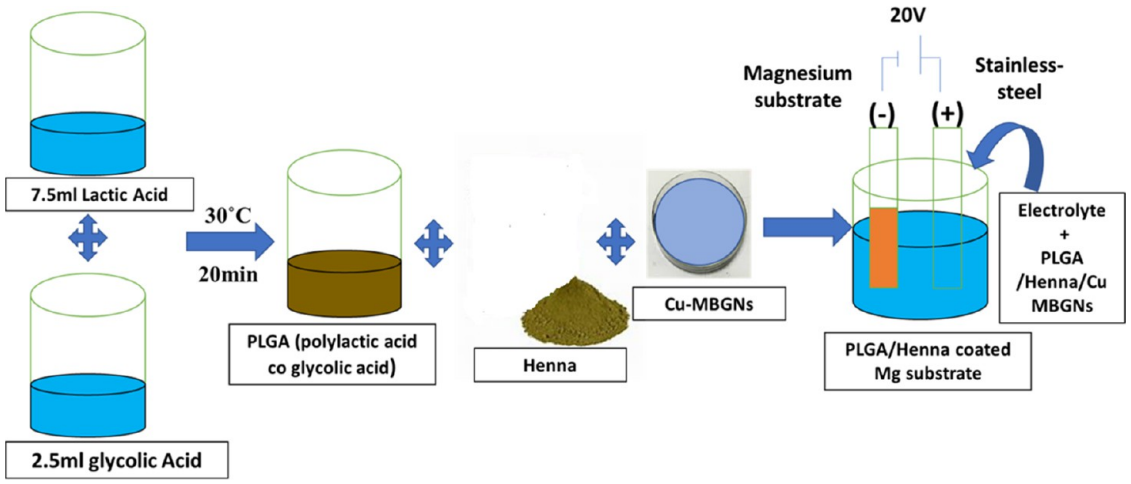

Figure 3. Schematic illustration for the electrophoretic deposition of PLGA/henna/Cu-MBGNs on the Mg substrate (cathode). Coated samples were cut by a saw very carefully for different characterizations.

deposition voltage parameters were optimized, as shown in Table 1. Figure 3 depicts a schematic representation of the entire EPD process.

2.7. Characterization of PLGA/Henna/Cu-MBGNs Composite Coatings. *2.7.1. ζ-Potential.* Using a nano zeta sizer (Malvern Instruments, U.K.), the ζ-potential was measured to determine the colloidal suspension stability via the laser Doppler velocimetry (LDV) technique. 0.1 g/L dilution was prepared for the solid suspension content for accurate measurements. The values were taken in triplicates at 25 °C for PLGA, henna, and Cu-MBGNs within the pH range of 2.0−10.0.

2.7.2. Ion Release in PBS. Inductively coupled plasma optical emission spectroscopy (ICP-OES, PerkinElmer Optima 8300) was used to analyze the ion release of Cu-MBGNs incorporated in composite coatings. The ions released from Cu-MBGNs/PLGA/henna in a phosphate-buffered saline (PBS) medium were measured over 14 days. Cu-MBGNs-doped composite coatings (<1 μm) were soaked in 50 mL of PBS. 5 mL of absorbing medium was taken out daily to analyze the ion release behavior of Cu-MBGNs, followed by the addition of 5 mL of fresh PBS back to the immersion solution. The sample was incubated at 37 °C with an agitation speed of 120 rpm. During ion release studies, internal standards containing scandium were used as reference standards to avoid nonspectral interferences and achieve precision, following a previous study.[37] The results for triplicates of all dissolved ions with average values and standard deviations were reported. The cumulative release of calcium, silicon, and copper ions as a function of time was analyzed.

2.7.3. Brunauer−Emmett−Teller (BET) Analysis. BET Analysis was carried out to obtain the full isotherm using a V-Sorb 2800P BET surface area and porosimetry analyzer. First, the samples were degassed at 120 °C for 60 min to remove any contaminants from their surfaces. The samples were then subjected to specific heating conditions in a vacuum or an inert gas environment. The surface area was determined at −196 °C by combining N_2 and He physical adsorption in the relative pressure range of 0.00−0.35. BET pore size distribution and pore volume were also determined. The isotherms obtained were then classified following the International Union of Pure and Applied Chemistry (IUPAC).

2.7.4. Scanning Electron Microscopy (SEM)/Energy-Dispersive Spectroscopy (EDX) Analysis. A field emission scanning electron microscope investigated the surface topography and morphological analysis of composite coatings deposited on Mg substrates (FE-SEM, MIRA, TESCAN). Then, the composite coating's qualitative elemental composition (at an acceleration voltage of 15 kV) was carried out using an energy-dispersive X-ray spectroscope (EDX) equipped with SEM. The samples were sputtered with gold by Q150/ S (Quorum Technologies) in order to eliminate the charging effect during analysis. The sputtering thickness was ∼5 nm.

2.7.5. Fourier Transformation Infrared (FTIR) Analysis. The functional groups in PLGA/henna/Cu-MBGNs coatings were characterized using an attenuated total reflection Fourier transformation infrared (ATR-FTIR) spectroscope (Thermo-Fisher Nicolet Summit Pro) equipped with OMNIC paradigm software. The transmittance spectrum was obtained in the 4000−400 cm^{-1} range at a resolution of 4 cm^{-1}.

2.7.6. Adhesion Test. 2.7.6.1. Tape Test. The adhesion strength of composite coatings (n = 5) deposited on Mg substrates was determined using a tape test. A crosshatch adhesion test was conducted according to the ISO 2409 and ASTM D3359-17 standards.[38,39] Scratches were formed on the coated substrates using a CC2000 basic crosshatch cutter. The adhesive tape was then placed over the substrate for 90 s and then removed at 180° from the surface. The scratches were then compared to ASTM D3359 standards to determine the quality of the adhesion strength.[40,41]

2.7.6.2. Bend Test. The bending strength of composite coatings with dimensions of 60 mm × 30 mm × 0.5 mm was determined using the bend test by following the ASTM B571-97 standard (n = 5).[42] The composite-coated sample was bent at an angle of 180° by the plier. In order to assess the adhesive strength of composite coatings, the delamination and deformation capabilities of the coating were observed. The deformed samples following the bending test were evaluated using an M50 stereomicroscope.

2.7.7. Contact Angle Test. The surface wettability of the composite coatings and the bare Mg substrate was measured using deionized water droplets (5 μL). The droplet was dropped on composite-coated Mg substrates and bare Mg samples using a microliter pipette (n = 5). A digital camera was used to take the image after every 5 s. Afterward, the images

https://doi.org/10.1021/acsomega.3c01384
ACS Omega 2023, 8, 18074−18089

were analyzed via Image J software. To ensure the accuracy of the results, the mean and standard deviations were computed.

2.7.8. Surface Roughness. A stylus profilometer (TMR 360) was used to measure the bare Mg sample's average surface roughness (R_a) and PLGA/henna/Cu-MBGNs-coated substrates. The granite reference plane supports the measured samples. The microscopic tip moves horizontally with profile length of 5 mm while remaining in contact with the surface. The R_a of the composite coatings and bare Mg substrates was then analyzed.

2.7.9. Corrosion Behavior. The Gamry instrument (reference 600) Potentiostate was used to investigate the corrosion behavior of the composite coatings and bare substrates. In order to perform corrosion studies, the coated samples were cut into 10 mm × 10 mm (square shape) by using an EDM machine. Further, the edges and backside of the coated sample and the uncoated sample were insulated by magic depoxy steel (made in Pakistan). Samples were then dried for 1 h. The total area that was exposed during electrochemical testing was 1 cm^2. The Gamry instrument was equipped with a three-electrode cell, in which coated/uncoated substrates act as working electrodes, graphite as a counter electrode, and Ag/AgCl as a reference electrode.

The corrosion study was performed at 37 °C using simulated body fluid (SBF). Potentiodynamic polarization scans were conducted at a 2.5 mV/s scan rate over a potential range of ±500 mV. The Tafel plot was extrapolated to determine the corrosion potential (E_{corr}) and the corrosion current density (I_{corr}). The test was performed 3 times. The EIS test was performed at open circuit potential with a 10 mV perturbation. The frequency ranged from 100 kHz to 1 mHz. Every measurement was performed at least three times.

2.7.10. In Vitro Bioactivity. *In vitro* bioactivity of the composite coatings was investigated using SBF, which was prepared by following Kokubo et al.[43] The composite coatings were immersed in 50 mL of SBF and then incubated at 37 °C in an Orbital shaking incubator (30 rpm) for 1, 7, and 21 days. The SBF was refreshed after 24 h to replicate the physiological conditions. At each time interval, samples were collected, rinsed with fresh water, and then stored in a desiccator. Before and after immersion in SBF, samples were analyzed using SEM, and FTIR analysis and X-ray diffraction (XRD) investigations (D8 Advance, Bruker) were utilized to confirm HA layer formation in SBF.

2.7.11. Antibacterial Test. Composite-coated Mg substrates of dimension 1 cm × 1 cm (square shape) were used to analyze the antibacterial effect via an agar disk diffusion test. In antibacterial studies, the whole surface of the sample was coated. 15 μL overnight cultured bacterial strains (*Escherichia coli* and *Staphylococcus aureus* with 0.015 ± 0.02 (OD_{600}) optical density) were poured over two 15 mL agar Petri dishes to create a uniform bacterial lawn. The samples were UV-sterilized for 30 min. Afterward, the coated side of the samples was placed over agar plates and incubated at 37 °C for 24 h (coatings should be in direct contact with the agar plate). A digital camera was used to take the images of the plates after 24 h. The images were then analyzed via Image J software to measure the zone of inhibition. The test was repeated 5 times for each type of sample, and the mean values along with standard deviation were reported.

The antibacterial efficacy of the composite coatings was tracked quantitatively using the colony-forming unit (CFU) assay. Nutrient broth (Oxoid-U.K.) was used to culture both *S. aureus* and *E. coli* independently. 10 mL of infusion was prepared by adding 10 μL of stock bacterial strains. The control (bare Mg) and PLGA/henna/Cu-MBGNs-coated Mg samples were dipped in the prepared infusions and incubated at 37 °C for 24 h in an Orbital shaker. The said test tubes were centrifugated at 11,000 rpm, and 1 mL of supernatant was separated. 5 μL of stock bacteria were reintroduced and incubated again for 24 h. Potentization was done, and then, 100 μL from each dilution was transferred to solid medium plates. The viable colonies were inspected and counted visually.

2.7.12. Cell Culture. MG-63 Osteoblast cells (CRL1427, ATCC, Manassas, VA) originally isolated from a human sarcoma were used to evaluate the cytocompatibility of the coatings using the WST-8 assay. PLGA/henna and PLGA/henna/Cu-MBGN-coated disc-shaped (having a diameter of 13 mm) Mg substrates were used for cell studies. In cell culture studies, we opted for the disc-shaped samples in contrast to other material characterizations. The reason was that in cell biology studies we used a 24-well plate to house the samples and the disc-shaped samples with 13 mm diameter fit in nicely. The uncoated Mg substrate was used as a control sample. Dulbecco's modified Eagle's medium (DMEM), supplemented with 10 vol % fetal bovine serum (FBS; Gibco) and 1 vol % penicillin/streptomycin (Pen-Strep; Gibco), was used to prepare the cell culture medium. The prepared medium was then transferred to a 75 cm^2 canted-neck cell culture flask (SPL Life Sciences), and osteoblast cells were added. To reach 80−90% confluence, the culture medium carrying osteoblast cells was placed in a CO_2 incubator (NUAIRE) with 5% CO_2, 37 °C, and a humid atmosphere for 48 h. The used medium was discarded, and grown cells were washed with phosphate-buffered saline (PBS; Gibco). Subsequently, the cells were trypsinized with 0.25% trypsin/EDTA (Trypsin-EDTA; Gibco) to detach cells from the walls of the canted-neck cell culture flask. The cells were dyed with trypan blue (Sigma-Aldrich), and live cells were counted in a hemocytometer. On the other hand, samples were placed in a 24-well plate and sterilized under UV light for 1 h. In cell culture studies, different sterilization times were selected keeping in view the difference in the sample size (13 mm) and shape (disc) compared to that of the antibacterial studies. 867 μL of cell suspension, including 10^5 cells/mL, was added to each sample. The number of living cells was counted using a hemocytometer by introducing trypan blue dye (Sigma-Aldrich). The samples containing cells were sterilized in a 24-well plate under UV light for 1 h. A 24-well plate was then placed in the incubator for 48 h with 5% CO_2, humidity more than 85% at 37 °C temperature, and cells were allowed to grow on both control and coated samples. The WST-8 (water-soluble tetrazolium salt) test was performed to quantify the cell viability. Following standard protocols (Cell counting kit 8: Sigma-Aldrich), the used cell culture medium was replaced with 400 μL of fresh DMEM solution containing 1% WST-8 reagent in each well coursed by the standards mentioned above of incubation.

The absorbance value of the uncoated Mg sample (control) was taken as 100% cell viability. The viability of the culture plates with coated samples was measured against the control. The experiment results (done in triplicate) were stated as the mean value ± standard deviation (SD). Moreover, one-way analysis of variance (ANOVA) with $p < 0.05$, $p < 0.001$, and $p < 0.001$ was deployed for statistical analysis, while Tukey's

https://doi.org/10.1021/acsomega.3c01384
ACS Omega 2023, 8, 18074−18089

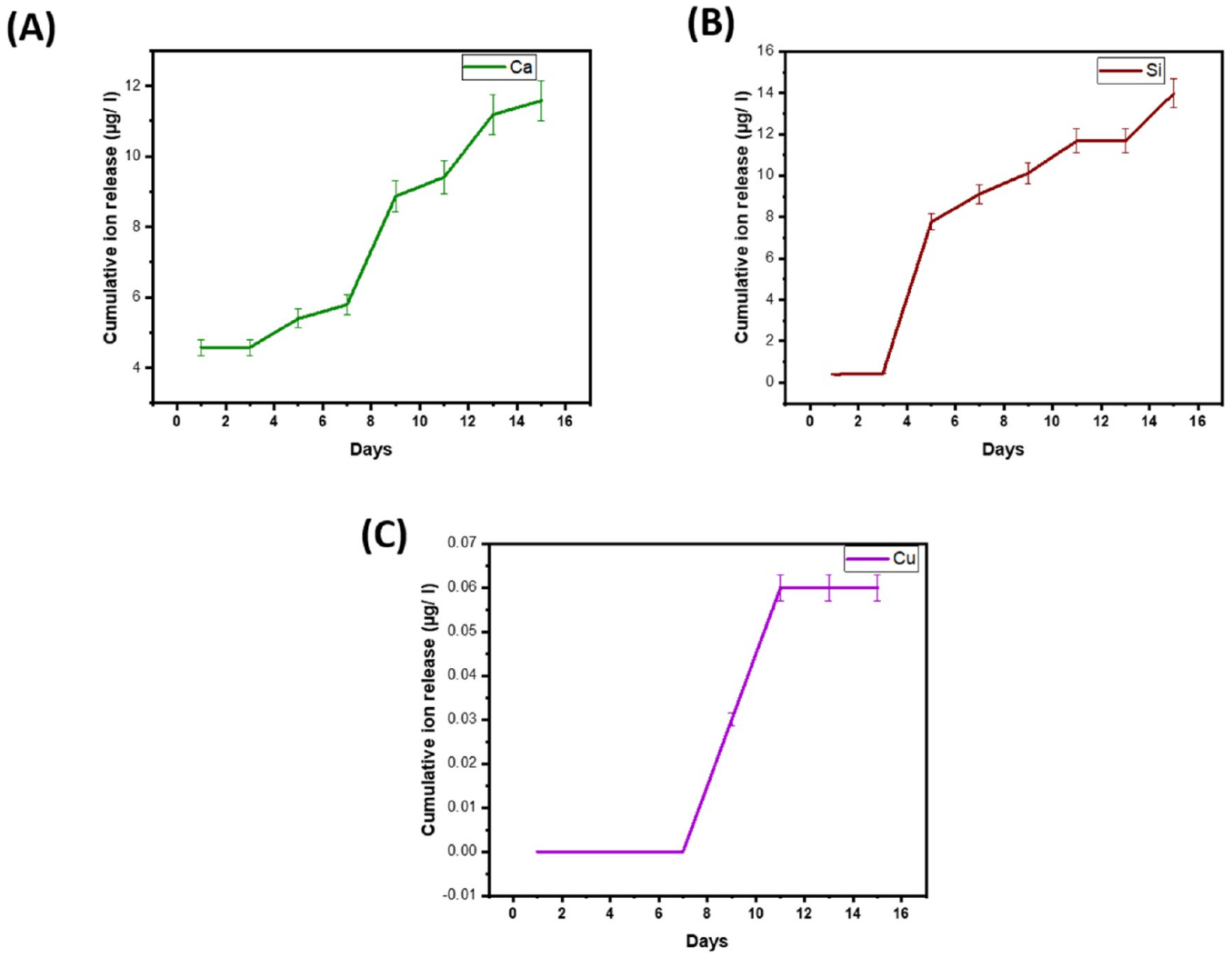

Figure 4. Ionic concentrations of (A) Ca, (B) Si, and (C) Cu released into PBS from composite coatings after refreshing the solutions and at different time intervals (1, 7, and 14 days).

range test was utilized (the study was carried out using statistical software; MINITAB 16) for post hoc analysis.

3. RESULTS AND DISCUSSION

3.1. ζ-Potential. ζ-potential was measured to assess the stability of the suspension as a function of pH; intermolecular forces play an essential role in attractive and repulsive forces between dispersed particles of the suspension. PLGA (8 vol %) and henna (2 g/L) showed negative ζ-potentials, i.e., (−10 ± 4 mV) and (−12 ± 3 mV), respectively, which is in agreement with the literature.[44,45] The addition of henna to PLGA changed the surface chemistry of the suspension. PLGA and henna were negatively charged at a pH of 4.5 due to the presence of hydroxyl groups, exerting repulsive forces (F_R) on each other. Furthermore, the blend suspension contained H^+ ions of PLGA and OH^- ions of henna, due to which electrostatic attractive forces (F_A) were created between PLGA and henna to form a polyelectrolyte complex (PLGA/henna).[46] The attractive forces formed were not enough to overcome the strong repulsive forces. Consequently, suspension stability was achieved due to the strong electrostatic repulsive forces between PLGA and henna, where the blend suspension of PLGA and henna showed a negative ζ-potential (−9 ± 4 mV).

Adding Cu-MBGNs to the PLGA/henna suspension yielded a positive ζ-potential (+18.4 ± 5) at a pH of 4.5. The positively charged Cu-MBGNs and negatively charged hydroxyl groups of PLGA/henna exhibited electrostatic attractive forces (F_A). The molecules of PLGA/henna were adsorbed on Cu-MBGNs due to these attractive electrostatic forces (F_A). The adsorption and strong interaction between PLGA/henna and Cu-MBGNs were achieved for the codeposition of PLGA/henna/Cu-MBGNs.[47] Therefore, the polyelectrolyte complex (PLGA/henna) and the Cu-MBGNs migrate toward the cathode under the application of an electric field due to the positive ζ-potential.[48]

3.2. Ion Release. The ion release behavior of Ca^{+2}, Si^{+4}, and Cu^{+2} ions from the composite coatings is shown in Figure 4. The cumulative ion release (PPM) was determined upon immersion of coatings in PBS for 14 days. The antibacterial activity, angiogenic activity, and in vitro bioactivity of the immersed coatings were evaluated in relation to the ion release profile. Figure 4 depicts the variation in Ca, Si, and Cu concentrations over time. The release of Si ions indicates the dissolution of MBGNs. Figure 4A shows the release of Ca ions in the first 14 days, which may lead to the bioactivity of the

https://doi.org/10.1021/acsomega.3c01384
ACS Omega 2023, 8, 18074−18089

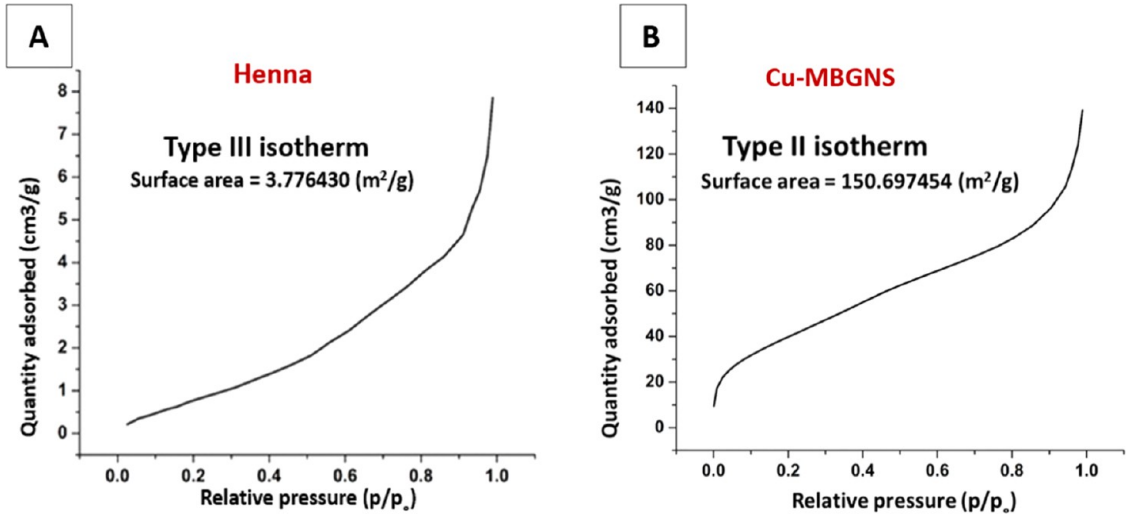

Figure 5. Nitrogen adsorption isotherms of (A) henna and (B) Cu-MBGNs.

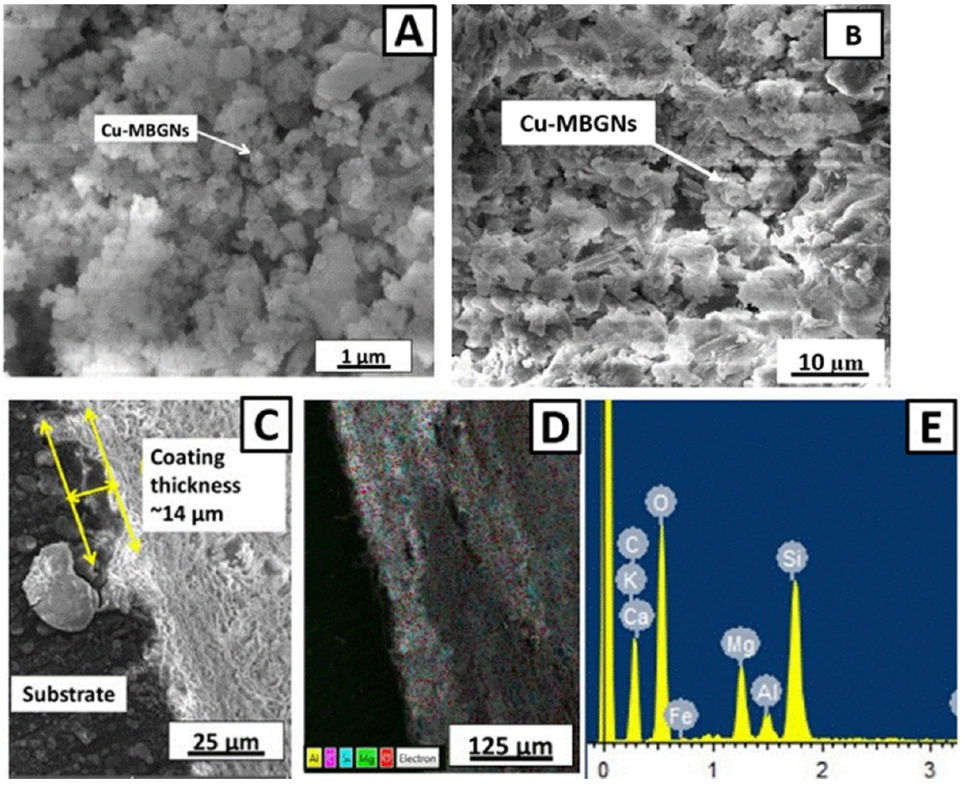

Figure 6. SEM images and EDX analysis of Mg coated with PLGA/henna/Cu-MBGN composite coatings. (A, B) Morphology of Cu-MBGNs embedded in PLGA/henna/Cu-MBGN composite coatings at different magnifications. (C) Cross-sectional SEM image of PLGA/henna/Cu-MBGN composite coatings. (D) EDX mapping showing elements of Mg, C, Si, and Al. (E) EDX spectrum of PLGA/henna/Cu-MBGN composite coatings.

composite coatings. However, these results contradict with those in the existing literature.[37] A burst release of Si ions was observed in the first week of incubation, while the release of the ions decreased in the following week (Figure 4B). Notably, the release of Si ions will have positive long-term bioactivity effects in bone regeneration, as well as antibacterial and angiogenic effects.[49] According to Rocton et al.,[50] the concentration of Si ions increases due to the dissolution of MBGNs. In contrast, the concentration of Ca decreases due to the formation of calcium phosphate during the first 2 weeks (Figure 4A). Figure 4C shows the low release of Cu ions during the first week, followed by a burst release during the second week. However, the cumulative release of Cu ions is still low after 2 weeks. In a few instances, the release of Cu ions was less than 1 PPM (below the precision limit of the machine). Thus, the detection of Cu release is not accurate in the current study. The reason for the less release of Cu ions is that the Cu-MBGNs is incorporated in the polymeric matrix, which may lead to the slow release of Cu ions. Further, the small amount of Cu in MBGNs could also be the reason.

The release rates of Si and Ca ions are in agreement with those of Westhauser et al.[51] Further, the release of Si and Ca

https://doi.org/10.1021/acsomega.3c01384
ACS Omega 2023, 8, 18074−18089

ions was sufficient to induce in vitro bioactivity, as illustrated in Section 3.10. The release of Si and Ca ions can help the implant material to form a bond with the host tissues.[36] Moreover, the release of ions from the composite coatings was not high enough to induce toxicity to the osteoblast cell line, as illustrated in the cell culture studies (Section 3.12). However, the release of Cu ion was <1 PPM, which is quite low. The higher release of Cu ions may induce toxicity; therefore, the controlled release of Cu ions is important. In the current study, the release of Cu ions was not high to cause toxicity. Therefore, we can conclude that the release of Cu, Si, and Ca ions was appropriate to gain targeted therapeutic effects, as illustrated in the in vitro bioactivity, antibacterial studies, and cell culture studies.

3.3. BET Analysis of PLGA/Henna/Cu-MBGNs Composite Coatings. The surface area and porosity of henna and Cu-MBGNs were evaluated using BET analysis (Figure 5). Figure 5 shows the nitrogen adsorption isotherm of henna and Cu-MBGNs. BET analysis of henna shows a type III isotherm, i.e., a multilayer adsorption isotherm with a surface area of 3.776 m^2/g (Figure 5A). When the pressure rises, the adsorption uptake increases exponentially until the relative pressure approaches unity. The activated carbon and water pair at 30 °C to form a Type-IV isotherm, as shown in Figure 5B. At low pressure, the adsorption surface was immediately saturated. The adsorption uptake occurs at higher pressures, exhibiting an exponential increase resulting in the development of multilayer adsorption. The Type-IV isotherm indicated the mesopore porosity in MBGNs with a surface area of 102 m^2/g. Figure 5B displays the experimental data for the isotherm and the inhibited adsorption uptake from the suggested universal adsorption model. A nonsymmetrical single peak energy distribution graph for a Type-IV isotherm demonstrates the creation of many layers, which corresponds to the capillaries being filled. Near a relative pressure of unity, the adsorption comes to an end.

The surface areas of henna and Cu-MBGNs are 3.776 and 102 m^2/g, respectively. The small surface area of henna relative to Cu-MBGNs in the developed coatings confirms the macroporous structure. Thus, it demonstrates the possibility of incorporating henna within the pores of Cu-MBGNs. The large surface area of Cu-MBGNs also ensures the mesoporous structure of the developed coatings.

3.4. SEM Analysis of PLGA/Henna/Cu-MBGN Composite Coating. SEM was used to confirm the surface morphology, homogeneity, and uniformity of PLGA/henna/Cu-MBGNs composite coatings deposited on Mg substrates using EPD. The surface of the composite coating looks relatively homogeneous (Figure 6A), showing well-distributed Cu-MBGNs particles, most probably due to the colloidal stability of the suspension. Figure 6B shows that Cu-MBGNs are embedded in the PLGA/henna, resulting in a densely packed coating morphology. Similar coating morphologies were reported for PLGA coatings on Mg substrates.[27,52] The cross-sectional SEM image of the PLGA/henna/Cu-MBGNs composite coating confirms the uniformity of the coating with a coating thickness of ∼14 μm (Figure 6C). The elemental mapping of the PLGA/henna/Cu-MBGNs composite coating indicates the presence of Al, Si, Mg, and C (Figures 6D,E), confirming that all elements of composite coating constituents are present within the microstructure. Table 2 demonstrates the elemental composition of Mg coated with PLGA/henna/Cu-MBGNs composite coating. As EDX analysis may lead to misleading results (as the detection of C and O via EDX is not accurate), FTIR analysis is presented in the following section to verify the presence of PLGA, henna, and Cu-MBGNs in the composite coating.

Table 2. EDX Analysis of Mg Coated with PLGA/Henna/Cu-MBGN Composite Coatings

sr. no.	element	composition (wt %)
1	C	39.50
2	O	47.38
3	Mg	6.13
4	Al	0.40
5	Si	4.67
6	S	0.41
7	K	0.49
8	Ca	0.89
9	Cu	0.03

3.5. FTIR of PLGA/Henna/Cu-MBGN Composite Coatings. FTIR spectra of Cu-MBGNs, henna, and PLGA/henna/Cu-MBGNs are shown in Figure 7A. The FTIR spectra of Cu-MBGNs showed Si−O−Si symmetric vibrations and Cu−O stretching at ∼990 and ∼600 cm^{-1}, respectively.[53,54] The FTIR spectra of PLGA showed a C−H stretching peak at ∼2990 cm^{-1}. In addition, the peak of the carbonyl group (C═O) appeared at ∼1750 cm^{-1} due to the presence of two monomers, i.e., PLA and PGA. Furthermore, the peak at ∼980 cm^{-1} was attributed to C−O stretching in PLGA.[29] The FTIR spectra of henna showed an O−H bond peak at ∼3320 cm^{-1}.[25] The carbonyl group (C═O) and aliphatic C−H stretching peaks appeared at ∼1755 and ∼2925 cm^{-1}, respectively. The peak at ∼1000 cm^{-1} was attributed to the C−OH phenolic group in henna.[55]

The FTIR spectrum of the PLGA/henna/Cu-MBGN composite coating is displayed in Figure 7B. The spectra showed C−H stretching, C−O stretching, and carbonyl group (C═O) peaks of PLGA at ∼2980, ∼1750 cm^{-1}, and ∼985 cm^{-1}, respectively.[30] Furthermore, the Cu−O stretching peak of Cu-MBGNs appeared at 1010 cm^{-1}.[53] The peaks at ∼3250 cm^{-1} indicated the O−H bond of henna.[25] Overall, the FTIR analysis confirmed the presence of PLGA, henna, and Cu-MBGNs in the composite coatings.

3.6. Adhesion Test of PLGA/Henna/Cu-MBGN Composite Coating. *3.6.1. Tape Test.* A tape test was carried out on PLGA/henna/Cu-MBGNs composite coatings to qualitatively assess the adhesion strength between the Mg substrate and the composite coatings (Figure 8A,B). The composite coating displayed minimal delamination (<5%). According to ASTM D3359 standards, the adhesion strength was rated as "4B", proving that the coating has suitable adhesion strength for orthopedic applications.[2,56]

3.6.2. Bend Test. Deformability of PLGA/henna/Cu-MBGNs composite coating was evaluated by a bend test described in the ASTM in B571-97 (Figure 8C). The coating was observed after bending for any possible imperfections using a stereomicroscope. The coatings possess sufficient resistance to bending loads in the center of the substrate, where the bending stress is maximum, indicative of a high flexural strength. The coating adheres firmly to the Mg substrate without any sign of delamination.

3.7. Contact Angle Measurements. Initial protein and cellular attachment is highly dependent on the wettability, surface roughness, and surface chemistry of deposited coatings,

https://doi.org/10.1021/acsomega.3c01384
ACS Omega 2023, 8, 18074−18089

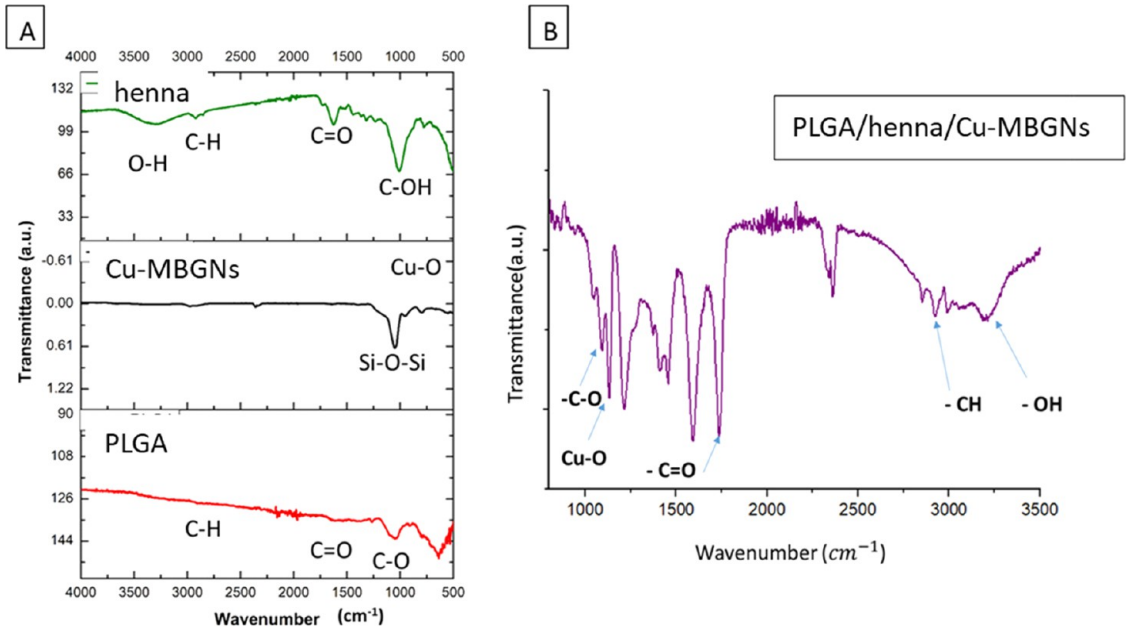

Figure 7. FTIR spectra of (A) henna, Cu-MBGNs, and PLGA and (B) PLGA/henna/Cu-MBGN coating on the Mg substrate.

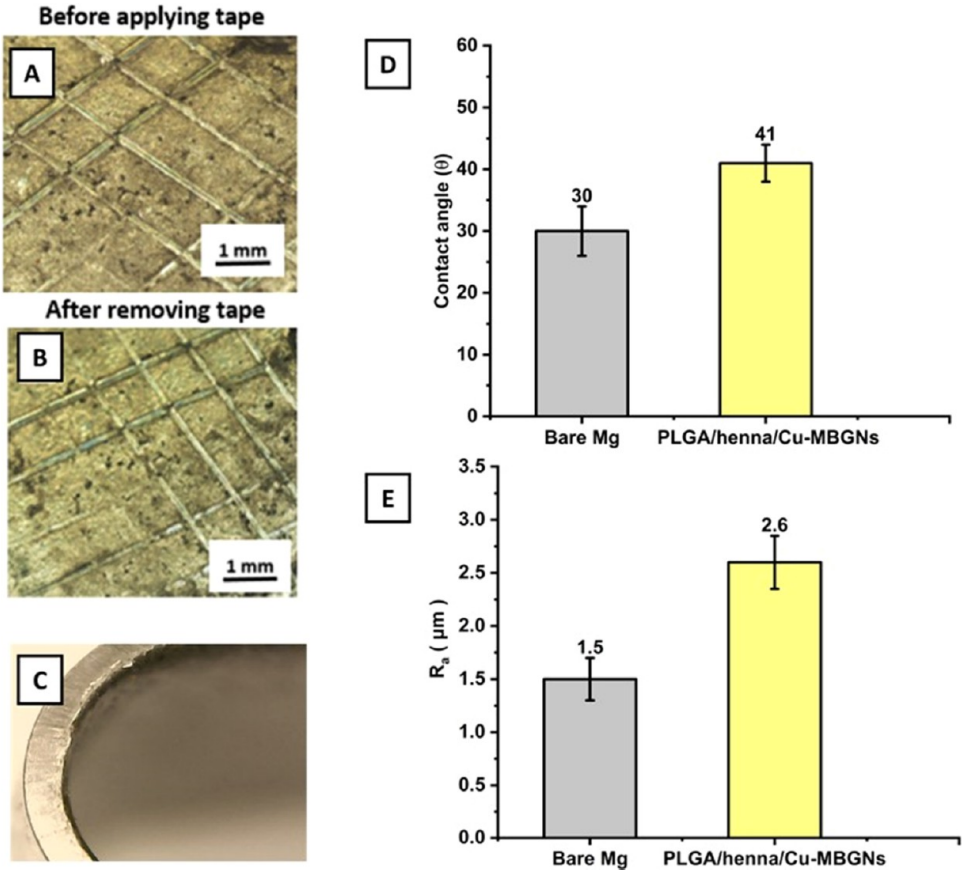

Figure 8. Stereomicroscope images showing the result of the tape test; (A) before applying the tape, (B) after removing the tape, and (C) digital camera showing the results of the bend test. (D) Contact angle measurement results and (E) surface roughness measurement results for pure Mg and Mg coated with PLGA/henna/Cu-MBGNs, where error bars indicate the standard deviation where $n = 3$.

the optimal combination of which determines the implant's suitability.[57] More particularly, the wettability of the coating surface significantly influences the initial accumulation of the protein, which determines the adhesion behavior of osteoblast cells.[58] Thus, the contact angles of bare Mg and PLGA/henna/Cu-MBGNs composite coating deposited on Mg substrates were evaluated in this section. The contact angle of the composite coating lies within a superior wettability range of 35−80° for initial protein attachment (Figure 8D).[59] Figure 8D demonstrates that the coated and uncoated Mg substrates

https://doi.org/10.1021/acsomega.3c01384
ACS Omega 2023, 8, 18074−18089

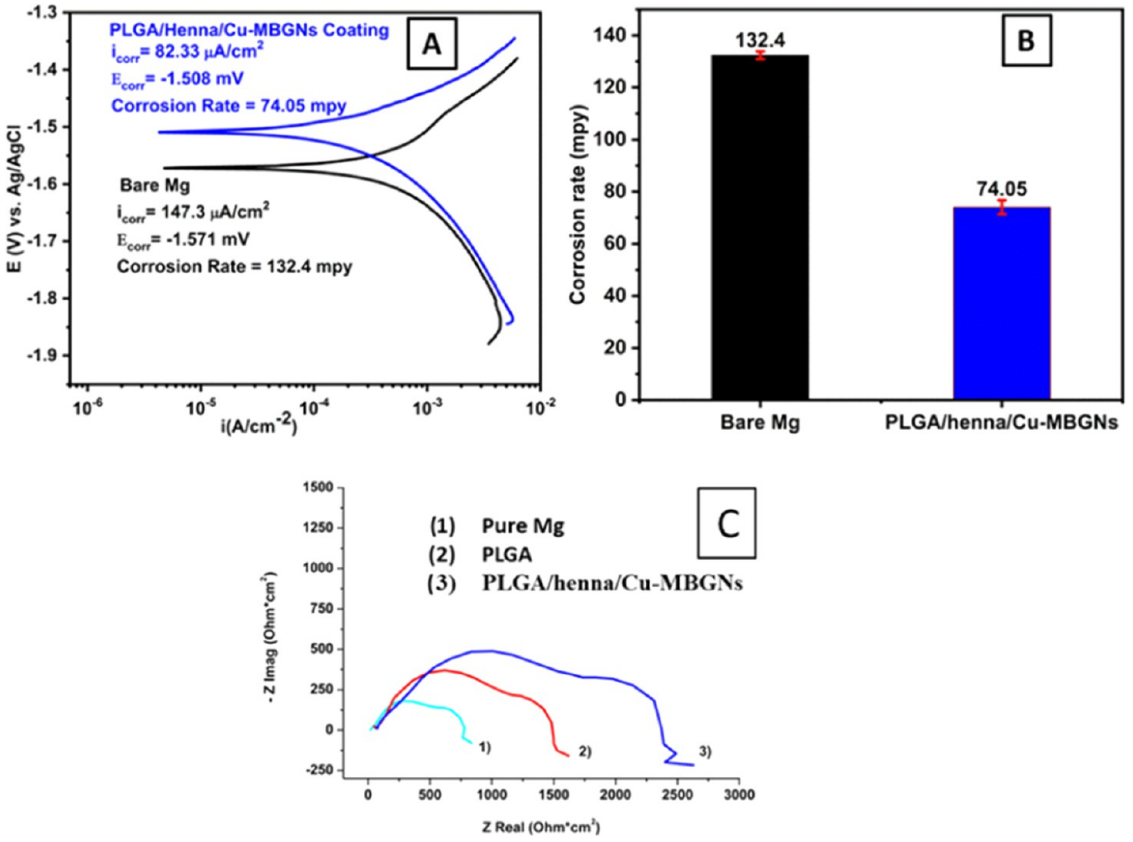

Figure 9. (A) Comparison of Tafel plots of bare Mg and composite coatings of PLGA/henna/Cu-MBGNs deposited on Mg substrates. (B) Comparison of the corrosion rate of bare Mg and composite-coated Mg substrates. (C) Nyquist plot of pure Mg, PLGA-coated Mg, and PLGA/henna/Cu-MBGN-coated Mg.

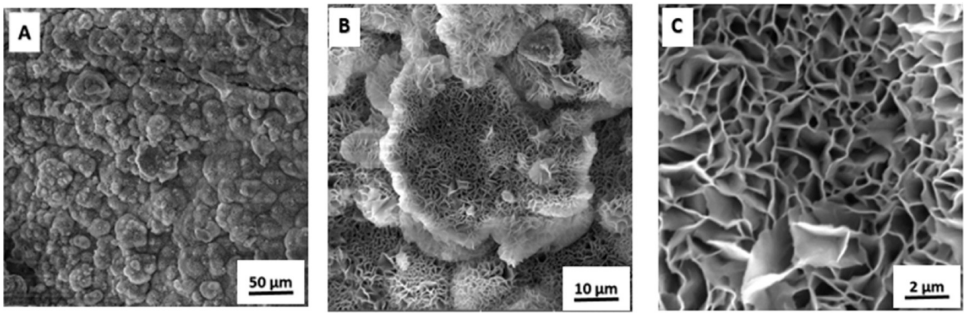

Figure 10. SEM images of PLGA/henna/Cu-MBGNs after immersion in SBF for 21 days at different magnifications (A) at 100×, (B) at 2500×, and (C) at 50k×.

lie within the hydrophilic range, indicating good wettability and agreeing well with the literature.[33]

3.8. Surface Roughness Measurements. In addition to wettability, surface topography is also essential for determining the response of the surface toward cellular interaction, as stated previously.[60,61] Therefore, the average surface roughness (R_a) was measured on bare Mg and PLGA/henna/Cu-MBGNs composite coatings for comparison. The measured values of R_a for bare Mg and composite coating on Mg are 1.5 and 2.6 μm, respectively, as shown in Figure 8E.

3.9. Corrosion Behavior of PLGA/Henna/Cu-MBGN Composite Coating. Figure 9A illustrates the potentiodynamic polarization (PDP) scan to investigate the ability of PLGA/henna/Cu-MBGNs composite coating deposited on Mg substrates to control the degradation rate of Mg. This technique is the most-used electrochemical technique to study in vitro corrosion. The bare Mg sample has $E_{corr} \sim -1.571$ V, while the composite coating has $E_{corr} \sim -1.508$ V. The bare Mg and PLGA/henna/Cu-MBGNs composite-coated samples have almost similar E_{corr} but display a significantly different i_{corr} due to a shift in anodic kinetics. The corrosion rate of PLGA/henna/Cu-MBGNs composite samples was also evaluated (Figure 9). In comparison to bare Mg, Mg coated with PLGA/henna/Cu-MBGNs showed a ~2 order of magnitude decrease of the corrosion rate. Consequently, the coated sample demonstrated reduced corrosion current density (as illustrated in Figure 9A), which is crucial for biomaterials.[61] Figure 9B shows the comparison of corrosion rates along with the error bars representing the standard deviation. The impedance was measured from an initial time (t = 0), immediately after the

https://doi.org/10.1021/acsomega.3c01384
ACS Omega 2023, 8, 18074−18089

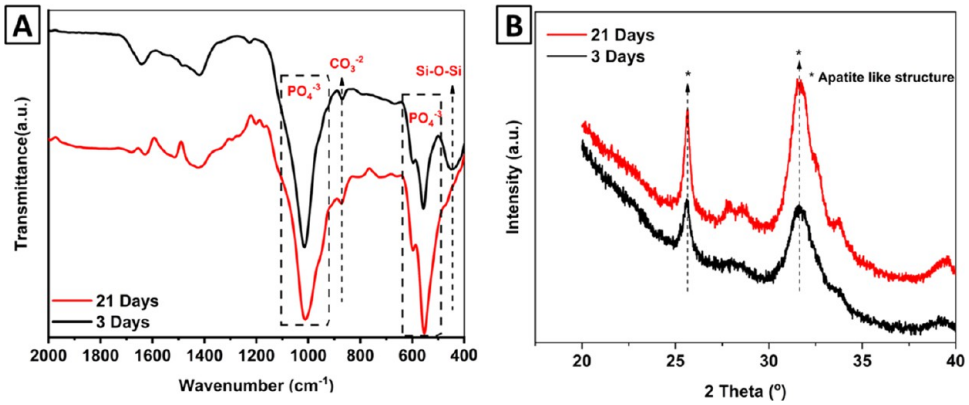

Figure 11. HA layer formation on PLGA/henna/Cu-MBGN coatings after immersion in SBF for 3 and 21 days: (A) FTIR spectra and (B) XRD spectra for 3 and 21 days.

Table 3. Inhibition Zone Data of PLGA/Cu-MBGN and PLGA/Henna/Cu-MBGN Coatings against *E. coli* and *S. aureus* (n = 5)

sample	inhibition zone against *S. aureus* (cm)	sample diameter (cm)	inhibition zone against *E. coli* (cm)	sample diameter (cm)
control (PLGA/Cu-MBGNs)	na	1.7	na	1.5
composite coating (PLGA/henna/Cu-MBGNs)	1.7 ± 0.2	1.4	2.3 ± 0.3	1.7

stabilization of the potential. The Nyquist plot of all of the curves is illustrated in Figure 9C, which indicates the formation of an oxide layer on the surface of the pure Mg substrate, wherein the second and third circles (i.e., PLGA coating on Mg and PLGA/henna/Cu-MBGNs coating on Mg) showed a significantly higher increase in impedance than the coatings. Figure 9C confirms that the PLGA/henna/Cu-MBGNs coating increased the impedance more than the PLGA coating alone. Recently, Ahmad et al.[62] found that the polymeric coatings (Zein) can improve the corrosion resistance of the substrate material. The polymeric coatings act as barrier layers and impede the flow of the physiological fluid toward the substrate, thus slowing the corrosion and degradation kinetics.

3.10. In Vitro Bioactivity of PLGA/Henna/Cu-MBGN Composite Coating. Bioactivity is an important characteristic of biomaterials that forms the interface between implants and biological tissues.[63] Therefore, an in vitro bioactivity test was performed by immersing PLGA/henna/Cu-MBGNs samples in SBF for 21 days. The formation of the HA layer on the composite coating was confirmed through SEM, EDX, FTIR, and XRD analyses. Following that, samples were removed from the SBF, and SEM images were captured. After immersion in SBF for 21 days, PLGA/henna/Cu-MBGNs coating developed a cauliflower-like structure on their surfaces (Figure 10), which is an indication of the formation of hydroxyapatite (HA) crystals.[64] The Ca/P ratio of the formed layer was 1.64 (calculated via EDX analysis), which is close to the stoichiometric ratio of HA.

Higher-magnification images reveal a nanostructured hydroxyapatite layer (Figures 10B,C), where the plate-like structure corresponds to the coenriched HA crystals,[65] confirming the bioactivity of the composite coating deposited on Mg substrates.

FTIR analysis of composite coatings after immersion in SBF also confirmed the formation of the apatite-like structure. The immersion of Cu-MBGNs containing composite coatings in SBF resulted in the dissolution of glass particles, releasing calcium and silicate ions into the solution. These ions reacted with the SBF, leading to the formation of a supersaturated solution of calcium phosphate, which ultimately resulted in the nucleation and growth of HA crystals on the coating surface. Specifically, the disappearance of the Si−O−Si stretching peak associated with bioactive glass was observed in the FTIR spectra after 21 days, which previously appeared at 443 cm^{-1}.[25] Furthermore, the appearance of carbonate (873 cm^{-1}) and phosphate (562 and 601 cm^{-1}) peaks can be attributed to carbonated HA formation (Figure 11A).[23]

An X-ray diffraction (XRD) investigation was performed on PLGA/henna/Cu-MBGNs coating after immersion in SBF to confirm the presence of the hydroxyapatite (HA) layer (Figure 11 B). The XRD analysis confirmed the formation of the HA layer after immersion in simulated body fluid (SBF) for 3 and 21 days. The diffraction pattern showed peaks associated with the HA at 25.8 and 31.7° (JCPDS Card#9-0432).[23]

The formation of the HA layer on the surface of the composite coatings refers that the implant can form a bond with the natural bone/tissue. The composite coatings developed an HA layer on their surface allowing the further growth of HA (which is a bone-like material), which will fill in the gap at the fracture site and will bond with natural bone. The ability of the material to form a bond with the natural bone is termed as "in vitro bioactivity".[36,66] The reason for the improved bioactivity is attributed to the nanoscale Cu-MBGNs on the top surface of the coatings providing rapid ion exchange between the coatings and the physiological environment.[36]

3.11. Antibacterial Test. The antibacterial efficacy of the composite coating is essential to prevent biofilm formation. Thus, the antibacterial activity of composite coatings was evaluated against *E. coli* (Gram-negative bacteria) and *S. aureus* (Gram-positive bacteria) by the disk diffusion method. The disc diffusion test was repeated five times (n = 5) for each type of sample, and the mean values for the zone of inhibition along with the standard deviation were reported (Table 3). The composite coating exhibits antibacterial activity, as evidenced

https://doi.org/10.1021/acsomega.3c01384
ACS Omega 2023, 8, 18074−18089

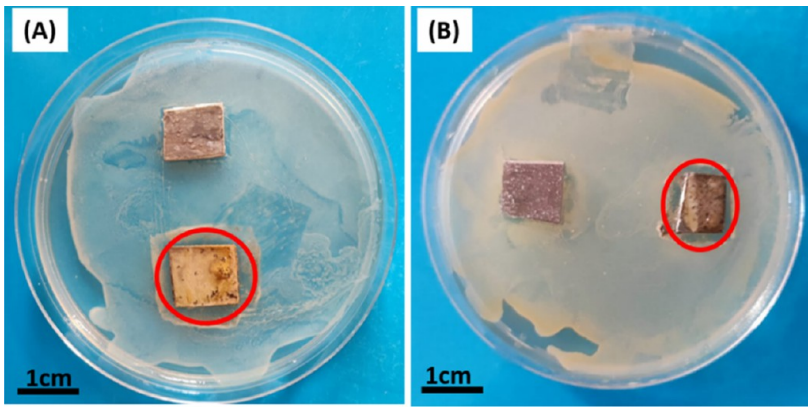

Figure 12. Antibacterial activity results of the composite coating against (A) *E. coli* and (B) *S. aureus*.

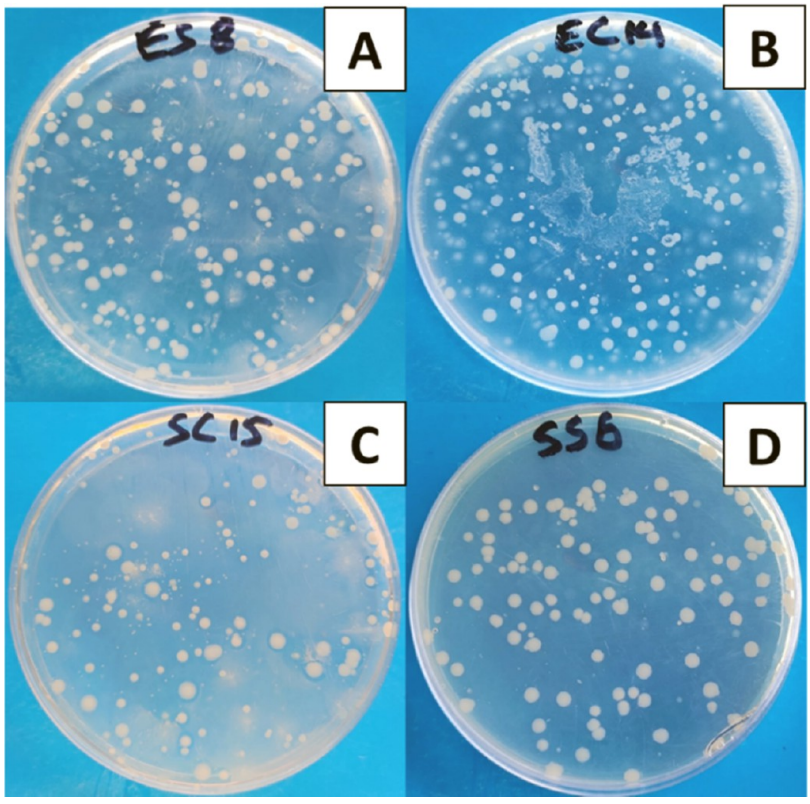

Figure 13. Results of CFU assay: (A) control (Mg) against *E. coli*, (B) PLGA/henna/Cu-MBGN coatings deposited on Mg against *E. coli*, (C) control against *S. aureus*, and (D) PLGA/henna/Cu-MBGN coatings deposited on Mg against *S. aureus*.

by the formation of a zone of inhibition against *E. coli* and *S. aureus* (Figure 12). The PLGA/henna/Cu-MBGNs coating developed a clear zone of inhibition against *E. coli* and *S. aureus*, while the control samples showed no zone of inhibition. Table 3 shows the measured values for the zones of inhibition with standard deviations where the composite coating shows significant antibacterial activity against Gram-positive bacteria than the Gram-negative bacteria. Similar results were reported where a significant zone of inhibition against Gram-positive bacteria was formed due to the incorporation of henna into different polymer-based coatings.[24,67] The antibacterial activity of henna is attributed to *Lawsone* (2-hydroxy-1,4-naphthoquinone) and flavonoids, which can interact with the bacterial cell wall and enzyme active sites to kill bacterial entities.[68] Additionally, the release of Cu ions from composite coatings also contributes to the antibacterial effect of the composite coatings, as stated in the literature.[54,69] Therefore, the improved antibacterial activity of the PLGA/henna/Cu-MBGNs composite coating against *E. coli* and *S. aureus* in the present study is attributed to the synergistic effect of henna and Cu-MBGNs.

In the CFU assay, the control (bare Mg substrate) and PLGA/henna/Cu-MBGNs coating deposited on Mg show a countable range of colonies at the 14th and 8th dilutions, respectively, against *E. coli* (Figure 13A,B). Contemporarily, the sample with PLGA/henna/Cu-MBGNs coating deposited on Mg exhibited a countable range at an earlier dilution, i.e., 6th dilution, and complete inhibition at the 8th dilution against *S. aureus* compared to the control (the control exhibited a partial inhibition at the 15th dilution and complete inhibition at the 18th dilution), as shown in Figure 13C,D. Furthermore, the growth of *E. coli* was inhibited partially at the 14th dilution

https://doi.org/10.1021/acsomega.3c01384
ACS Omega 2023, 8, 18074−18089

Table 4. PLGA/Henna/Cu-MBGN Coatings Deposited on Mg and Bare Mg (Control) CFU Test Evaluated from Cultured Plates against *E. coli* and *S. aureus*

		colony-forming units (CFU/mL)								
		dilution factor								
bacterial strain	sample	10^{-1} to -5	10^{-6}	10^{-7}	10^{-8}	10^{-9} to -13	10^{-14}	10^{-15}	10^{-15}	10^{-16}
E. coli	bare Mg	TNTC	TNTC	TNTC	TNTC	TNTC	2.04×10^{17}	TFTC		
E. coli	coated sample	TNTC	TNTC	TNTC	1.76×10^{11}	TFTC				
S. aureus	bare Mg	TNTC	TNTC	TNTC	TNTC	TNTC	TNTC	9.8×10^{17}	TNTC	
S. aureus	coated sample	TNTC	1.14×10^{9}	TFTC						

and completely at the 16th dilution against bare Mg, while PLGA/henna/Cu-MBGNs coating deposited on Mg inhibited partially at the 8th dilution and complete inhibition was observed at the 10th dilution (against *E. coli*). Colony-forming units from each plate were calculated and are given in Table 4.

3.12. Cell Culture. The cellular activity of PLGA/henna and PLGA/henna/Cu-MBGNs coating on the Mg substrate was examined using a WST-8 assay based on the percentage of cell viability. The viability of osteoblast cells on PLGA/henna and PLGA/henna/Cu-MBGNs coated on Mg substrates is shown in Figure 14. Both the coatings promoted the proliferation and growth of osteoblast cells in the initial incubation period of 48 h. There was no significant difference between the coatings with and without Cu-MBGNs and the control (Mg substrate) at $p < 0.05$. Additionally, PLGA/henna coatings exhibited a higher percentage of cell viability than the PLGA/henna/Cu-MBGNs coating. However, it may be inferred from comparing it to the control samples that incorporation of Cu-MGBNs into PLGA/henna does not significantly promote cell growth but is also not cytotoxic. Additionally, the Cu-MBGNs-coated Mg substrate exhibited a cell viability percentage that was nearly identical to that of the control sample (uncoated Mg substrate). Bioactive motifs linked to coatings alter the number of bonds between osteoblast cell integrins and peptides, thus affecting cell proliferation and integration.[27,70] The results of cell viability studies confirmed that the composite coatings are highly biocompatible, which agrees well with the previous results reported on PLGA and PLGA-based composite coatings.[26,71]

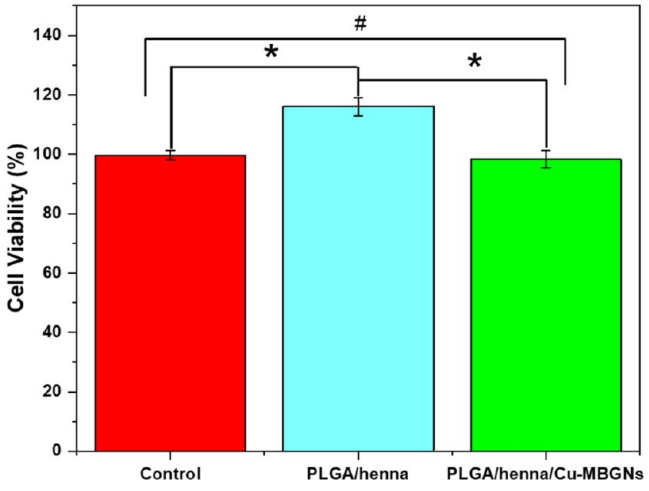

Figure 14. MG-63 cells' response to (1) uncoated Mg (control), (2) PLGA/henna coatings, and (3) PLGA/henna/Cu-MBGN coatings. The (*) shows that the difference between PLGA/henna and control, PLGA/henna, and PLGA/henna/Cu-MBGNs is statistically significant at $p < 0.05$ (data represents ± standard deviation of three samples), and (#) shows that the difference between control and PLGA/henna/Cu-MBGNs is statistically insignificant at $p < 0.05$ (data represents ± standard deviation of three samples).

In cell culture studies, we reported the results after 48 h of incubation since the cytotoxic effect is expected due to the relatively higher release of ions (Cu) and henna from the composite coatings. The release of Cu ions is significantly higher after 48 h of incubation and still the composite coatings exhibited cytocompatible behavior. In addition, we also conducted the cell culture studies by using WST-8 after 24 h of incubation. The results of the cell viability study after 24 and 48 h of incubation were quite similar, and we reported the results after 48 h of incubation to illustrate that the coatings were cytocompatible even after longer exposure times.

In the future, it would be interesting to conduct the cell culture studies for extended time periods. Furthermore, cell morphology and spreading can also be investigated to better understand the interaction between the cells and the surface of the coatings. The release of henna from the composite coatings would also help in understanding the cell biology and antibacterial behavior of the composite coatings. Moreover, cell mineralization (such as Alizarin red staining) can give detailed information on the bioactivity of the composite coatings.

In this study, we opted to deposit composite coatings on the Mg substrate rather than the surface modification of Mg. Surface modification can also help improve the biological properties such as reduced inflammatory response and better cell attachment.[72] However, surface coatings in the case of Mg is a better choice because composite coatings can effectively control the degradation kinetics of Mg for biomedical applications. However, in the future, it would be interesting to study the combination of surface modifications and surface coating to improve the biological response in addition to controlling the degradation.

4. CONCLUSIONS

PLGA/henna/Cu-MBGNs composite coatings were deposited on Mg via EPD. The results demonstrated that uniform coatings of PLGA/henna/Cu-MBGNs were deposited on the Mg substrate under optimum EPD parameters. The composite coatings facilitated the attachment and proliferation of osteoblast cells through suitable wettability and surface topography. The release of henna and Cu (ions) from composite coatings provided an antibacterial effect. The composite coatings presented suitable adhesion strength and corrosion resistance for orthopedic applications. Furthermore, the composite coatings exhibited suitable bioactivity for bone tissue engineering applications. The overall results showed that the PLGA/henna/Cu-MBGNs composite coating is suitable to control the corrosion rate of Mg-based orthopedic implants

https://doi.org/10.1021/acsomega.3c01384
ACS Omega 2023, 8, 18074−18089

and to inhibit the formation of the biofilm. The results of the current study confirm that the PLGA/henna/Cu-MBGNs composite coatings can be considered for in vivo trials and eventually clinical applications.

■ ASSOCIATED CONTENT

Data Availability Statement

The data sets used and/or analyzed during the current study are available from the corresponding author upon reasonable request.

Supporting Information

The Supporting Information is available free of charge at https://pubs.acs.org/doi/10.1021/acsomega.3c01384.

Coating combined FTIR; corrosion studies after coatings; CuAgMBGNs; CuAg-MBGNs BET; CuAg-MBGNs BJH adsorption; CuAg-MBGNs BJH desorption, and CuAg-MBGNs BJH isotherm (ZIP)

■ AUTHOR INFORMATION

Corresponding Author

Muhammad Atiq Ur Rehman − *Department of Materials Science & Engineering, Institute of Space Technology Islamabad, Islamabad 44000, Pakistan;* orcid.org/0000-0001-5201-973X; Email: atique1.1@hotmail.com

Authors

Jawad Manzur − *Department of Materials Science & Engineering, Institute of Space Technology Islamabad, Islamabad 44000, Pakistan*

Memoona Akhtar − *Department of Materials Science & Engineering, Institute of Space Technology Islamabad, Islamabad 44000, Pakistan*

Aqsa Aizaz − *Department of Materials Science & Engineering, Institute of Space Technology Islamabad, Islamabad 44000, Pakistan*

Khalil Ahmad − *Department of Materials Science & Engineering, Institute of Space Technology Islamabad, Islamabad 44000, Pakistan*

Muhammad Yasir − *Department of Materials Science & Engineering, Institute of Space Technology Islamabad, Islamabad 44000, Pakistan*

Badar Zaman Minhas − *Department of Materials Science & Engineering, Institute of Space Technology Islamabad, Islamabad 44000, Pakistan*

Egemen Avcu − *Department of Mechanical Engineering, Kocaeli University, Kocaeli 41001, Turkey; Ford Otosan Ihsaniye Automotive Vocational School, Kocaeli University, Kocaeli 41650, Turkey*

Complete contact information is available at: https://pubs.acs.org/10.1021/acsomega.3c01384

Notes

The authors declare no competing financial interest.

■ ACKNOWLEDGMENTS

This research was funded by Innovative and Collaborative Research under Pakistan U.K. Education Gateway (ICRG-2020) [Reference No: 006326/D/ISB/007/2021].

■ REFERENCES

(1) Ahmed, Y.; Yasir, M.; Ur Rehman, M. A. Fabrication and Characterization of Zein/Hydroxyapatite Composite Coatings for Biomedical Applications. *Surfaces* **2020**, *3*, 237−250.

(2) Batool, S. A.; Ahmad, K.; Irfan, M.; Ur Rehman, M. A. Zn−Mn-Doped Mesoporous Bioactive Glass Nanoparticle-Loaded Zein Coatings for Bioactive and Antibacterial Orthopedic Implants. *J. Funct. Biomater.* **2022**, *13*, No. 97.

(3) Nickells, J.; Georgiou, A.; Walton, B.Paper 3. In *SAQs for the Final FRCA*; Cambridge University Press, 2010; pp 23−24.

(4) Hench, L. L.; Thompson, I. Twenty-First Century Challenges for Biomaterials. *J. R. Soc. Interface* **2010**, *7*, S379−S391.

(5) Eliaz, N. Corrosion of Metallic Biomaterials: A Review. *Materials* **2019**, *12*, No. 407.

(6) Goldmann, W. H. Biosensitive and Antibacterial Coatings on Metallic Material for Medical Applications. *Cell Biol. Int.* **2021**, *45*, 1624−1632.

(7) Awais, M.; Aizaz, A.; Nazneen, A.; ul Ain Bhatti, Q.; Akhtar, M.; Wadood, A.; Ur Rehman, M. A. A Review on the Recent Advancements on Therapeutic Effects of Ions in the Physiological Environments. *Prosthesis* **2022**, *4*, 263−316.

(8) Rahmati, M.; Stötzel, S.; El Khassawna, T.; Iskhahova, K.; Wieland, D. C. F.; Plumhoff, B. Z.; Haugen, H. J. Early Osteoimmunomodulatory Effects of Magnesium-Calcium-Zinc Alloys. *J. Tissue Eng.* **2021**, *12*, No. 204173142110471.

(9) Mansoorianfar, M.; Mansourianfar, M.; Fathi, M.; Bonakdar, S.; Ebrahimi, M.; Zahrani, E. M.; Hojjati-Najafabadi, A.; Li, D. Surface Modification of Orthopedic Implants by Optimized Fluorine-Substituted Hydroxyapatite Coating: Enhancing Corrosion Behavior and Cell Function. *Ceram. Int.* **2020**, *46*, 2139−2146.

(10) Dzobo, K.; Thomford, N. E.; Senthebane, D. A.; Shipanga, H.; Rowe, A.; Dandara, C.; Pillay, M.; Shirley, K.; Motaung, C. M. Innovation and Transformation of Medicine. *Stem Cells Int.* **2018**, *2018*, 1−24.

(11) Ur Rehman, M. A.; Bastan, F. E.; Haider, B.; Boccaccini, A. R. Electrophoretic Deposition of PEEK/Bioactive Glass Composite Coatings for Orthopedic Implants: A Design of Experiments (DoE) Study. *Mater. Des.* **2017**, *130*, 223−230.

(12) Pogorielov, M.; Husak, E.; Solodivnik, A.; Zhdanov, S. Magnesium-Based Biodegradable Alloys: Degradation, Application, and Alloying Elements. *Interventional Med. Appl. Sci.* **2017**, *9*, 27−38.

(13) Schwalfenberg, G. K.; Genuis, S. J. The Importance of Magnesium in Clinical Healthcare. *Scientifica* **2017**, *2017*, 1−14.

(14) Boccaccini, A. R.; Keim, S.; Ma, R.; Li, Y.; Zhitomirsky, I. Electrophoretic Deposition of Biomaterials. *J. R. Soc. Interface* **2010**, *7*, S581−S613.

(15) Woesz, A.; Best, S. M. *Cellular Response to Bioceramics*; Woodhead Publishing Limited, 2008; pp 136−155.

(16) Ferraris, S.; Yamaguchi, S.; Barbani, N.; Cazzola, M.; Cristallini, C.; Miola, M.; Vernè, E.; Spriano, S. Bioactive Materials: In Vitro Investigation of Different Mechanisms of Hydroxyapatite Precipitation. *Acta Biomater.* **2020**, *102*, 468−480.

(17) Florea, D. A.; Albuleţ, D.; Grumezescu, A. M.; Andronescu, E. Surface Modification − A Step Forward to Overcome the Current Challenges in Orthopedic Industry and to Obtain an Improved Osseointegration and Antimicrobial Properties. *Mater. Chem. Phys.* **2020**, *243*, No. 122579.

(18) Marín-Suárez, M.; Medina-Rodríguez, S.; Ergeneman, O.; Pané, S.; Fernández-Sánchez, J. F.; Nelson, B. J.; Fernández-Gutiérrez, A. Electrophoretic Deposition as a New Approach to Produce Optical Sensing Films Adaptable to Microdevices. *Nanoscale* **2014**, *6*, 263−271.

(19) Taye, M. B. Biomedical Applications of Ion-Doped Bioactive Glass: A Review. *Appl. Nanosci.* **2022**, *12*, 3797−3812.

(20) Westhauser, F.; Decker, S.; Nawaz, Q.; Rehder, F.; Wilkesmann, S.; Moghaddam, A.; Kunisch, E.; Boccaccini, A. R. Impact of Zinc- or Copper-Doped Mesoporous Bioactive Glass Nanoparticles on the Osteogenic Differentiation and Matrix

Formation of Mesenchymal Stromal Cells. *Materials* **2021**, *14*, No. 1864.
(21) Vu, A. A.; Bose, S. Natural Antibiotic Oregano in Hydroxyapatite-Coated Titanium Reduces Osteoclastic Bone Resorption for Orthopedic and Dental Applications. *ACS Appl. Mater. Interfaces* **2020**, *12*, 52383−52392.
(22) Virk, R. S.; Ur Rehman, M. A.; Munawar, M. A.; Schubert, D. W.; Goldmann, W. H.; Dusza, J.; Boccaccini, A. R. Curcumin-Containing Orthopedic Implant Coatings Deposited on Poly-Ether-Ether-Ketone/Bioactive Glass/Hexagonal Boron Nitride Layers by Electrophoretic Deposition. *Coatings* **2019**, *9*, No. 572.
(23) Ur Rehman, M. A.; Ferraris, S.; Goldmann, W. H.; Perero, S.; Bastan, F. E.; Nawaz, Q.; di Confiengo, G. G.; Ferraris, M.; Boccaccini, A. R. Antibacterial and Bioactive Coatings Based on Radio Frequency Co-Sputtering of Silver Nanocluster-Silica Coatings on PEEK/Bioactive Glass Layers Obtained by Electrophoretic Deposition. *ACS Appl. Mater. Interfaces* **2017**, *9*, 32489−32497.
(24) Asadi, H.; Suganthan, B.; Ghalei, S.; Handa, H.; Ramasamy, R. P. A Multifunctional Polymeric Coating Incorporating Lawsone with Corrosion Resistance and Antibacterial Activity for Biomedical Mg Alloys. *Prog. Org. Coat.* **2021**, *153*, No. 106157.
(25) Ur Rehman, M. A.; Bastan, F. E.; Nawaz, Q.; Goldmann, W. H.; Maqbool, M.; Virtanen, S.; Boccaccini, A. R. Electrophoretic Deposition of Lawsone Loaded Bioactive Glass (BG)/Chitosan Composite on Polyetheretherketone (PEEK)/BG Layers as Antibacterial and Bioactive Coating. *J. Biomed. Mater. Res., Part A* **2018**, *106*, 3111−3122.
(26) Tian, Q.; Rivera-Castaneda, L.; Liu, H. Optimization of Nano-Hydroxyapatite/Poly(Lactic-Co-Glycolic Acid) Coatings on Magnesium Substrates Using One-Step Electrophoretic Deposition. *Mater. Lett.* **2017**, *186*, 12−16.
(27) Li, L. Y.; Cui, L. Y.; Zeng, R. C.; Li, S. Q.; Chen, X. B.; Zheng, Y.; Kannan, M. B. Advances in Functionalized Polymer Coatings on Biodegradable Magnesium Alloys − A Review. *Acta Biomater.* **2018**, *79*, 23−36.
(28) Zhu, Y.; Liu, W.; Ngai, T. Polymer Coatings on Magnesium-Based Implants for Orthopedic Applications. *J. Polym. Sci.* **2022**, *60*, 32−51.
(29) So, H. N.; Hye, Y. N.; Jae, R. J.; In, S. B.; Park, J. S. Curcumin-Loaded PLGA Nanoparticles Coating onto Metal Stent by Electrophoretic Deposition Techniques. *Bull. Korean Chem. Soc.* **2007**, *28*, 397−402.
(30) Razzaghi, M.; Kasiri-Asgarani, M.; Bakhsheshi-Rad, H. R.; Ghayour, H. In Vitro Bioactivity and Corrosion of PLGA/Hardystonite Composite-Coated Magnesium-Based Nanocomposite for Implant Applications. *Int. J. Miner., Metall. Mater.* **2021**, *28*, 168−178.
(31) Baştan, F. E.; Ur Rehman, M.; Avcu, Y. Y.; Avcu, E.; Üstel, F.; Boccaccini, A. R. Electrophoretic Co-Deposition of PEEK-Hydroxyapatite Composite Coatings for Biomedical Applications. *Colloids Surf., B* **2018**, *169*, 176−182.
(32) Ahmed, Y.; Nawaz, A.; Virk, R. S.; Wadood, A.; Rehman, M. A. U. Fabrication and Characterization of Zein/Bioactive Glass (BG) Deposited on Pre-treated Magnesium via Electrophoretic Deposition. *Int. J. Ceram. Eng. Sci.* **2020**, *2*, 254−263.
(33) Ayyoob, M.; Kim, Y. J. Effect of Chemical Composition Variant and Oxygen Plasma Treatments on the Wettability of PLGA Thin Films, Synthesized by Direct Copolycondensation. *Polymers* **2018**, *10*, No. 1132.
(34) Goh, Y.-F.; Alshemary, A. Z.; Akram, M.; Kadir, M. R. A.; Hussain, R. Bioactive Glass: An in vitro Comparative Study of Doping with Nanoscale Copper and Silver Particles. *Int. J. Appl. Glass Sci.* **2014**, *5*, 255−266.
(35) Bano, S.; Yasir, M.; Niaz, A.; Wadood, A.; et al. Synthesis and Characterization of Silver − Strontium (Ag-Sr) Doped Mesoporous Bioactive Glass Nanoparticles. *Gels* **2021**, *7*, No. 34.
(36) Nawaz, A.; Bano, S. S. S.; Yasir, M.; Wadood, A.; Ur Rehman, M. A. Ag and Mn-Doped Mesoporous Bioactive Glass Nanoparticles Incorporated into the Chitosan/Gelatin Coatings Deposited on PEEK/Bioactive Glass Layers for Favorable Osteogenic Differentiation and Antibacterial Activity. *Mater. Adv.* **2020**, *1*, 1273−1284.
(37) Neščáková, Z.; Zheng, K.; Liverani, L.; Nawaz, Q.; Galusková, D.; Kaňková, H.; Michálek, M.; Galusek, D.; Boccaccini, A. R. Multifunctional Zinc Ion Doped Sol − Gel Derived Mesoporous Bioactive Glass Nanoparticles for Biomedical Applications. *Bioact. Mater.* **2019**, *4*, 312−321.
(38) ASTM D3359 Test Methods For Measuring Adhesion By Tape - Micom.
(39) Cross Hatch Adhesion Testers | Adhesion Testing | UK Dyne Testing.
(40) Lakshmi, R. V.; Basu, B. J. Fabrication of Superhydrophobic Sol−Gel Composite Films Using Hydrophobically Modified Colloidal Zinc Hydroxide. *J. Colloid Interface Sci.* **2009**, *339*, 454−460.
(41) *ASTM D3363-20*; ASTM International: West Conshohocken, PA, 2020. Standard Test Method for Film Hardness by Pencil Test.
(42) Practice, S. Standard Practice for Qualitative Adhesion Testing of Metallic Coatings 1 2014.
(43) Kokubo, T.; Takadama, H. How Useful Is SBF in Predicting in Vivo Bone Bioactivity? *Biomaterials* **2006**, *27*, 2907−2915.
(44) Daniel, S. C. G. K.; Mahalakshmi, N.; Sandhiya, J.; Nehru, K.; Sivakumar, M. Rapid Synthesis of Ag Nanoparticles Using Henna Extract for the Fabrication of Photoabsorption Enhanced Dye Sensitized Solar Cell (PE-DSSC). *Adv. Mater. Res.* **2013**, *678*, 349−360.
(45) Simon, L. C.; Stout, R. W.; Sabliov, C. Bioavailability of Orally Delivered Alpha-Tocopherol by Poly(Lactic-Co-Glycolic) Acid (PLGA) Nanoparticles and Chitosan Covered PLGA Nanoparticles in F344 Rats. *Nanobiomedicine* **2016**, *3*, No. 8.
(46) Ur Rehman, M. A.; Munawar, M. A.; Schubert, D. W.; Boccaccini, A. R. Electrophoretic Deposition of Chitosan/Gelatin/Bioactive Glass Composite Coatings on 316L Stainless Steel: A Design of Experiment Study. *Surf. Coat. Technol.* **2019**, *358*, 976−986.
(47) Peter, M.; Binulal, N. S.; Nair, S. V.; Selvamurugan, N.; Tamura, H.; Jayakumar, R. Novel Biodegradable Chitosan-Gelatin/Nano-Bioactive Glass Ceramic Composite Scaffolds for Alveolar Bone Tissue Engineering. *Chem. Eng. J.* **2010**, *158*, 353−361.
(48) Voron'ko, N. G.; Derkach, S. R.; Kuchina, Y. A.; Sokolan, N. I. The Chitosan-Gelatin (Bio)Polyelectrolyte Complexes Formation in an Acidic Medium. *Carbohydr. Polym.* **2016**, *138*, 265−272.
(49) Mancuso, E.; Bretcanu, O. A.; Marshall, M.; Birch, M. A.; McCaskie, A. W.; Dalgarno, K. W. Novel Bioglasses for Bone Tissue Repair and Regeneration: Effect of Glass Design on Sintering Ability, Ion Release and Biocompatibility. *Mater. Des.* **2017**, *129*, 239−248.
(50) Rocton, N.; Oudadesse, H.; Lefeuvre, B.; Peisker, H.; Rbii, K. Fine Analysis of Interaction Mechanism of Bioactive Glass Surface after Soaking in SBF Solution: AFM and ICP-OES Investigations. *Appl. Surf. Sci.* **2020**, *505*, No. 144076.
(51) Westhauser, F.; Wilkesmann, S.; Nawaz, Q.; Hohenbild, F.; Rehder, F.; Saur, M.; Fellenberg, J.; Moghaddam, A.; Ali, M. S.; Peukert, W.; Boccaccini, A. R. Effect of Manganese, Zinc, and Copper on the Biological and Osteogenic Properties of Mesoporous Bioactive Glass Nanoparticles. *J. Biomed. Mater. Res., Part A* **2021**, *109*, 1457−1467.
(52) Chen, J.-Y.; Chen, X.-B.; Li, J.-L.; Tang, B.; Birbilis, N.; Wang, X. Electrosprayed PLGA Smart Containers for Active Anti-Corrosion Coating on Magnesium Alloy AMlite. *J. Mater. Chem. A* **2014**, *2*, 5738−5743.
(53) Milkovic, L.; Hoppe, A.; Detsch, R.; Boccaccini, A. R.; Zarkovic, N. Effects of Cu-Doped 45S5 Bioactive Glass on the Lipid Peroxidation-Associated Growth of Human Osteoblast-like cells *in vitro*. *J. Biomed. Mater. Res., Part A* **2014**, *102*, 3556−3561.
(54) Hoppe, A.; Meszaros, R.; Stähli, C.; Romeis, S.; Schmidt, J.; Peukert, W.; Marelli, B.; Nazhat, S. N.; Wondraczek, L.; Lao, J.; Jallot, E.; Boccaccini, A. R. In Vitro Reactivity of Cu Doped 45S5 Bioglass Derived Scaffolds for Bone Tissue Engineering. *J. Mater. Chem. B* **2013**, *1*, 5659−5674.
(55) Ur Rehman, M. A.; Bastan, F. E.; Nawaz, Q.; Boccaccini, A. R. Electrophoretic Deposition of Lawsone Loaded Nanoscale Silicate

https://doi.org/10.1021/acsomega.3c01384
ACS Omega 2023, 8, 18074−18089

Glass / Chitosan Composite on PEEK / BG Layers. *ECS Trans.* **2018**, *82*, 45−50.
(56) Batool, S. A.; Liaquat, U.; Channa, I. A.; Gilani, S. J.; Makhdoom, M. A.; Yasir, M.; Ashfaq, J.; bin Jumah, M. N.; ur Rehman, M. A. Development and Characterization of Zein/Ag-Sr Doped Mesoporous Bioactive Glass Nanoparticles Coatings for Biomedical Applications. *Bioengineering* **2022**, *9*, No. 367.
(57) Avcu, E.; Yasemin, Y. Y.; Baştan, F. E.; Ur Rehman, M. A.; Üstel, F.; Boccaccini, A. R. Tailoring the Surface Characteristics of Electrophoretically Deposited Chitosan-Based Bioactive Glass Composite Coatings on Titanium Implants via Grit Blasting. *Prog. Org. Coat.* **2018**, *123*, 362−373.
(58) Hong, W.; Guo, F.; Chen, J.; Wang, X.; Zhao, X.; Xiao, P. Bioactive Glass−Chitosan Composite Coatings on PEEK: Effects of Surface Wettability and Roughness on the Interfacial Fracture Resistance and in Vitro Cell Response. *Appl. Surf. Sci.* **2018**, *440*, 514−523.
(59) Avcu, E.; Avcub, Y. Y.; Baştan, F. E.; Ur Rehman, M. A.; Üstel, F.; Boccaccini, A. R. Tailoring the Surface Characteristics of Electrophoretically Deposited Chitosan-Based Bioactive Glass Composite Coatings on Titanium Implants via Grit Blasting. *Prog. Org. Coat.* **2018**, *123*, 362−373.
(60) Ureña, J.; Tsipas, S.; Jiménez-Morales, A.; Gordo, E.; Detsch, R.; Boccaccini, A. R. Cellular Behaviour of Bone Marrow Stromal Cells on Modified Ti-Nb Surfaces. *Mater. Des.* **2018**, *140*, 452−459.
(61) Ur Rehman, M. A.; Bastan, F. E.; Nawaz, A.; Nawaz, Q.; Wadood, A. Electrophoretic Deposition of PEEK/Bioactive Glass Composite Coatings on Stainless Steel for Orthopedic Applications: An Optimization for in Vitro Bioactivity and Adhesion Strength. *Int. J. Adv. Manuf. Technol.* **2020**, *108*, 1849−1862.
(62) Ahmad, K.; Manzur, J.; Tahir, M.; Hussain, R.; Khan, M.; Wadood, A.; Avcu, E.; Rehman, M. A. U. Electrophoretic Deposition, Microstructure and Selected Properties of Zein/Cloves Coatings on 316L Stainless Steel. *Prog. Org. Coat.* **2023**, *176*, No. 107407.
(63) Pishbin, F.; Mouriño, V.; Gilchrist, J. B. B.; McComb, D. W. W.; Kreppel, S.; Salih, V.; Ryan, M. P. P.; Boccaccini, A. R. R. Single-Step Electrochemical Deposition of Antimicrobial Orthopaedic Coatings Based on a Bioactive Glass/Chitosan/Nano-Silver Composite System. *Acta Biomater.* **2013**, *9*, 7469−7479.
(64) Simchi, A.; Tamjid, E.; Pishbin, F.; Boccaccini, A. R. (2011). Recent Progress in Inorganic and Composite Coatings with Bactericidal Capability for Orthopaedic Applications. *Nanomedicine* **2011**, *7*, 22−39.
(65) Pishbin, F.; Mouriño, V.; Flor, S.; Kreppel, S.; Salih, V.; Ryan, M. P.; Boccaccini, A. R. Electrophoretic Deposition of Gentamicin-Loaded Bioactive Glass/Chitosan Composite Coatings for Orthopaedic Implants. *ACS Appl. Mater. Interfaces* **2014**, *6*, 8796−8806.
(66) Nawaz, A.; Ur Rehman, M. A. Chitosan/Gelatin-Based Bioactive and Antibacterial Coatings Deposited via Electrophoretic Deposition. *J. Appl. Polym. Sci.* **2021**, *138*, No. 50220.
(67) Ur Atiq, M.; Rehman, U.; Bastan, F. E.; Nawaz, Q.; Goldmann, W. H.; Maqbool, M.; Virtanen, S.; Boccaccini, A. R. Electrophoretic Deposition of Lawsone Loaded Bioactive Glass (BG)/ Chitosan Composite on Polyetheretherketone (PEEK)/ BG Layers as Antibacterial and Bioactive Coating. *J. Biomed. Mater. Res., Part A* **2018**, *1*, 3111−3122.
(68) Rahmoun, N. M.; Boucherit-Otmani, Z.; Boucherit, K.; Benabdallah, M.; Villemin, D.; Choukchou-Braham, N. Antibacterial and Antifungal Activity of Lawsone and Novel Naphthoquinone Derivatives. *Med. Mal. Infect.* **2012**, *42*, 270−275.
(69) Rath, S. N.; Brandl, A.; Hiller, D.; Hoppe, A.; Gbureck, U.; Horch, R. E.; Boccaccini, A. R.; Kneser, U. Bioactive Copper-Doped Glass Scaffolds Can Stimulate Endothelial Cells in Co-Culture in Combination with Mesenchymal Stem Cells. *PLoS One* **2014**, *9*, No. e113319.
(70) Fan, H.; Hu, Y.; Zhang, C.; Li, X.; Lv, R.; Qin, L.; Zhu, R. Cartilage Regeneration Using Mesenchymal Stem Cells and a PLGA−Gelatin/Chondroitin/Hyaluronate Hybrid Scaffold. *Biomaterials* **2006**, *27*, 4573−4580.
(71) Zhen, Z.; Xi, T. F.; Zheng, Y. F. *Surface Modification by Natural Biopolymer Coatings on Magnesium Alloys for Biomedical Applications*; Woodhead Publishing Limited, 2015; pp 310−333.
(72) Batool, F.; Özçelik, H.; Stutz, C.; Gegout, P.-Y.; Benkirane-Jessel, N.; Petit, C.; Huck, O. Modulation of Immune-Inflammatory Responses through Surface Modifications of Biomaterials to Promote Bone Healing and Regeneration. *J. Tissue Eng.* **2021**, *12*, No. 204173142110414.

https://doi.org/10.1021/acsomega.3c01384
ACS Omega 2023, 8, 18074−18089